Front. Chem. Sci. Eng. 2023, 17(6): 784–794
https://doi.org/10.1007/s11705-022-2278-4

RESEARCH ARTICLE

Enzyme@bismuth-ellagic acid: a versatile platform for enzyme immobilization with enhanced acid-base stability

Junyang Xu[1], Guanhua Liu[1,2], Ying He (✉)[1], Liya Zhou[1], Li Ma[1], Yunting Liu[1], Xiaobing Zheng[1,2], Jing Gao[1], Yanjun Jiang (✉)[1,2]

1 School of Chemical Engineering and Technology, Hebei University of Technology, Tianjin 300130, China
2 National-Local Joint Engineering Laboratory for Energy Conservation of Chemical Process Integration and Resources Utilization, Hebei University of Technology, Tianjin 300130, China

Abstract *In situ* encapsulation is an effective way to synthesize enzyme@metal–organic framework biocatalysts; however, it is limited by the conditions of metal–organic framework synthesis and its acid-base stability. Herein, a biocatalytic platform with improved acid-base stability was constructed via a one-pot method using bismuth-ellagic acid as the carrier. Bismuth-ellagic acid is a green phenol-based metal–organic framework whose organic precursor is extracted from natural plants. After encapsulation, the stability, especially the acid-base stability, of amyloglucosidases@bismuth-ellagic acid was enhanced, which remained stable over a wide pH range (2–12) and achieved multiple recycling. By selecting a suitable buffer, bismuth-ellagic acid can encapsulate different types of enzymes and enable interactions between the encapsulated enzymes and cofactors, as well as between multiple enzymes. The green precursor, simple and convenient preparation process provided a versatile strategy for enzymes encapsulation.

Keywords bismuth-ellagic acid, *in situ* encapsulation, enzyme@MOF biocomposites

1 Introduction

Enzymes are ideal biocatalysts for various industrial applications [1–3]. They are already being used as biocatalysts in industrial production applications and have become a major force in chemical manufacturing because they adhered to the development of green chemistry and atomic economy [4,5]. However, enzymes may be short-lived in biocatalytic applications, and their susceptibility to surrounding physicochemical conditions limits their practical application [6]. In addition, the inherent instability of enzymes poses a constant threat to their long-term storage and reuse. Modern advances in biotechnology have helped us obtain more efficient and robust enzyme catalysts; in particular, directed evolutionary techniques have greatly improved the activity and stability of biocatalysts [7,8]. However, such optimized biocatalytic systems generally suffer from insufficient economic feasibility and reusability, which is not in line with the development requirements of a green circular economy. Furthermore, enzyme immobilization can protect enzymes from inactivation and degradation, facilitating their isolation and recycling [9,10]. Therefore, enzyme immobilization is an effective method to expand the industrial applications of enzyme.

Metal–organic frameworks (MOFs) are special hybrid porous materials that have been widely developed class of carriers for enzyme immobilization in recent years [11–13]. Their fascinating physicochemical characteristics, such as large specific surface area, tunable pore size, abundant functional groups, and ease of modification, make them well-adapted to provide a stable microenvironment for enzymes via host-object interactions or limiting effects [14–16]. Research reports on enzyme@MOF biocomposites have increased exponentially in recent years [17–19]. However, limited by the nature of MOFs, enzyme@MOF complexes prepared using azolate ligands are usually unstable under weakly acidic conditions, while the assembly of carboxylic acid ligands is unstable under weakly basic conditions [20,21]. Thus, the design and development of a novel enzyme@MOF complex that can maintain stability under both weakly acidic and weakly base conditions to accommodate the diversity of enzymes is a pressing issue.

Polyphenols are organic molecules containing phenolic

Received August 28, 2022; accepted November 5, 2022

E-mails: heying1980@hebut.edu.cn (He Y.),
yanjunjiang@hebut.edu.cn (Jiang Y.)

hydroxyl groups widely found in plants [22,23]. Polyphenols can form metal-polyphenol networks through coordination between chelating ligands and metal ions, which are potential ligands for synthesizing of MOF-based materials [24]. Compared to carboxylic acid-based MOFs, phenol-based MOFs have higher chemical stability due to the higher pK_a of phenolic groups, effectively chelating metal ions [25,26]. Although phenol-based MOFs have good stability, only a few types have been developed so far. Selecting suitable rigid polyphenol molecules and controlling their porosity poses a challenge in the synthesis of phenol-based MOFs [27]. Ellagic acid (EA) is the building block of tannins, which are natural polyphenolic biomolecules. It has a centrally symmetric rigid molecular structure and has been used to prepare phenolic MOFs by combining with bismuth and zirconium ions [28]. MOFs composed of EA and bismuth ions have good biocompatibility and remarkable chemical stability, which provides a platform for the construction of universal enzyme@MOF complexes.

In this study, Bi-EA were used to construct enzyme@MOF complexes via an *in situ* synthesis process. After optimizing the synthesis conditions, Bi-EA was found to be suitable for encapsulating of various types of enzymes and enabling interactions between enzymes and cofactors as well as between multiple enzymes. Amyloglucosidases (AMG) was used as a model enzyme to verify the encapsulation performance of Bi-EA. The AMG@Bi-EA complexes retained high catalytic activity, had improved stability, and remained stable under weak acid or weak base conditions. In addition, the synthesis of enzyme@Bi-EA was consistent with the concept of green synthesis and sustainability, in which ligands were derived from plant extracts, and the synthesis was performed at ambient temperature and pressure without using organic solvents. This work provides an effective strategy for *in situ* enzyme encapsulation with improved acid-base stability and further promotes the application of MOFs in biocatalysis.

2 Experimental

2.1 Chemicals

Bismuth acetate and sodium acetate were purchased from Shanghai Maclin Biochemical Technology Co., Ltd. (Shanghai, China). EA, 2-morpholinoethanesulfonic acid (MES), *N*-(2-hydroxyethyl)piperazine-*N*′-methanesulfonic acid (HEPES), glucose dehydrogenase (GDH), horseradish peroxidase (HRP), and *p*-nitrophenyl palmitate were purchased from Shanghai Aladdin Biochemical Technology Co., Ltd. (Shanghai, China). AMG and glucose oxidase (GOx) were purchased from Shanghai Yuanye Bio-Technology Co., Ltd. (Shanghai, China). Lipase B from *Candida antarctica* (CALB) was purchased from Beijing Dingguo Changsheng Biotechnology Co. Ltd. (Beijing, China). Organophosphorus hydrolase (OPH) was purchased from Beijing Schengenbiya Bioengineering Technology Co., Ltd. (Beijing, China). Parathion-methyl was purchased from Dr. Ehrenstorfer GmbH (Augsburg, Germany). All other reagents were purchased from Beijing Mreda Technology Co., Ltd. (Beijing, China).

2.2 Synthesis of Bi-EA and AMG@Bi-EA

To synthesize of Bi-EA, 30 mg of bismuth acetate was dispersed into 10 mL of various buffer solutions with different pH levels to form a milky suspension under stirring conditions, and then 10 mg of EA was added. At this time, the solution immediately turned gray and gradually turned yellowish-green. After stirring and reacting at 25 °C for 5 h, the Bi-EA solid was collected, washed three times with deionized water, and freeze-dried for later use. The buffer solutions used in the preparation of Bi-EA were sodium acetate buffer (0.2 mol·L^{-1}, pH = 4–5), MES (0.2 mol·L^{-1}, pH = 6), and HEPES (0.2 mol·L^{-1}, pH = 7–8).

AMG@Bi-EA was prepared using a one-pot method. Typically, AMG (1 mg·mL^{-1}) was dissolved in acetate buffer (0.2 mol·L^{-1}, pH = 5), followed by the successive addition of bismuth acetate and EA. The complex was obtained after 5 h. The AMG@Bi-EA solution was prepared according to the optimum pH of AMG. Since the optimum pH of AMG was 4–5, acetate buffer was chosen as the reaction medium.

2.3 Determination of enzyme activity and kinetic parameters

The enzyme activity of free AMG and AMG@Bi-EA was calculated as the amount of reducing sugar released with water-soluble starch as a substrate. The enzyme dispersion (100 μL) was added to 900 μL of sodium acetate buffer (pH 5), then 1 mL of dextrinized starch (1 wt %) was added. The reaction was terminated by adding NaOH (1 mol·L^{-1}, 0.5 mL) after 5 min. A certain amount of reaction solution was diluted to 0.5 mL, then 0.5 mL of dinitrosalicylic acid (DNS) reagent was added and heated at 100 °C for 5 min. The absorbance value of the mixture was measured at 540 nm to calculate the reducing sugar content [29]. The initial reaction velocities of free AMG and AMG@Bi-EA were measured at different starch concentrations (0–80 g·L^{-1}), and the Michaelis constant (K_m) was obtained via nonlinear fitting.

2.4 Thermal stability, acid-base stability, reusability and storage stability of AMG@Bi-EA

Free AMG and AMG@Bi-EA were incubated at 60, 65,

70, 75, and 80 °C, and residual enzymatic activity was assayed at 10-min intervals. The deactivation mechanical parameters were calculated using the following formulae:

$$\ln\left(\frac{C_{E_t}}{C_{E_0}}\right) = -k_d t, \tag{1}$$

$$\frac{C_{E_t}}{C_{E_0}} = \frac{A_t}{A_0}, \tag{2}$$

where C_{E_0} represents the initial enzyme concentration, C_{E_t} represents the concentration of active enzyme at time t, t represents the incubation time, k_d represents the one-step inactivation constant or decay constant, and A_0 and A_t denote the initial activity and activity at any moment t, respectively.

The half-life ($t_{1/2}$) and D-value of AMG and AMG@Bi-EA were calculated as follows:

$$t_{\frac{1}{2}} = \frac{\ln 2}{k_d} = \frac{0.6931}{k_d}, \tag{3}$$

$$\text{D-value} = \frac{\ln 10}{k_d} = \frac{2.303}{k_d}. \tag{4}$$

The inactivation energies (E_d) of free AMG and AMG@Bi-EA were calculated using the Arrhenius equation, where A_d is the precursor factor of the Arrhenius equation.

$$k_d = A_d \exp\left(-\frac{E_d}{RT}\right). \tag{5}$$

Turbidity (optical density at 540 nm, OD_{540}) was used to characterize the stability of the materials after incubation in different buffers (pH 2–12). Briefly, AMG@Bi-EA (5 mg) was dispersed in buffers with different pH values. After complete dispersion via ultrasound, 200 μL of the dispersion was transferred to a 96-well plate, and the time-course OD_{540} was assayed using a microplate reader. The pH stability of AMG@Bi-EA was immersed in buffers with different pH values, and the residual activity was measured after 6 h of incubation.

Proteinase K treatment of AMG@Bi-EA was performed using the following procedure: 20 mg AMG@Bi-EA was incubated in 4 mL of MES (0.2 mol·L^{-1}, pH 6) for 1 h, then 5 mg proteinase K was added, and the solution was incubated for 3 h. For free AMG and AMG@ZIF-8, the protein content was consistent with that added in AMG@Bi-EA.

The reusability of AMG@Bi-EA was determined as follows: 100 μL of AMG@Bi-EA dispersion was added to 900 μL of sodium acetate buffer (pH 5), then 1 mL of dextrinized starch (1 wt %) was added. After 5 min of reaction, AMG@Bi-EA and the reaction solution was separated via centrifugation (8000 r·min^{-1}, 5 min). The supernatant was used to determine the enzymatic activity, and the solid catalyst was washed with fresh buffer and then used for the next cycle. Certain amounts of AMG@Bi-EA and AMG were dispersed in an aqueous solution, and the change in activity with time was measured to analyze their storage stability.

3 Results and discussion

3.1 Preparation and optimization of Bi-EA synthesis

The synthesis of Bi-EA hybrid materials was investigated under different pH conditions. The phase structure and morphologies of Bi-EA are shown in Fig. 1. As shown in Fig. 1(a), the synthesis of Bi-EA in the pH range of 4–7 was achieved by selecting a suitable buffer. The resulting materials were denoted as Bi-EA-*n*, where *n* represents

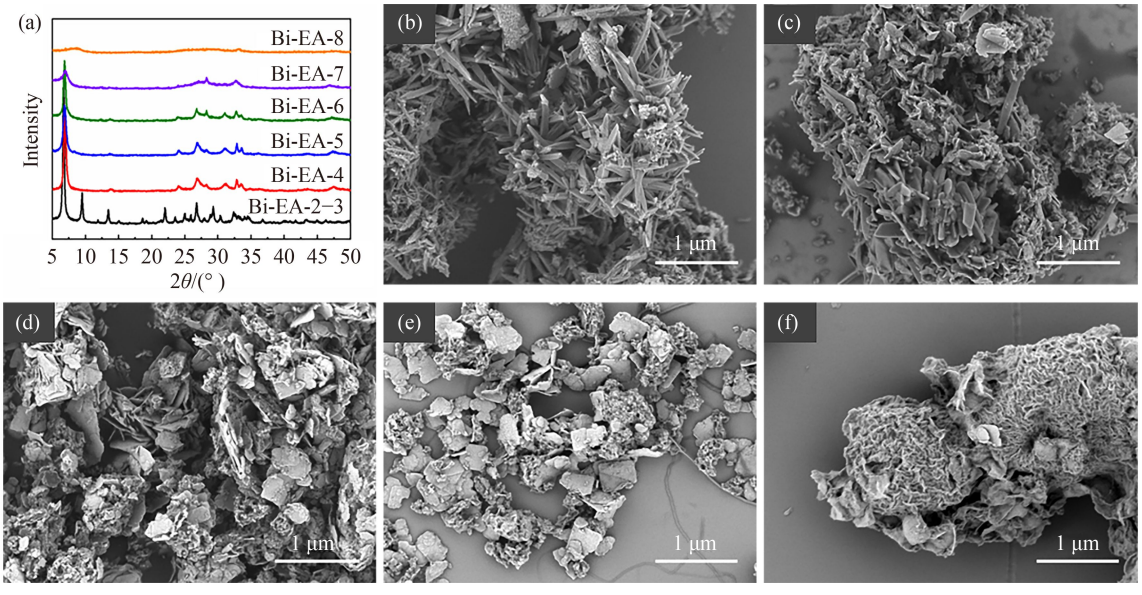

Fig. 1 (a) PXRD patterns and SEM images of (b) Bi-EA-3, (c) Bi-EA-4, (d) Bi-EA-5, (e) Bi-EA-6 and (f) Bi-EA-7.

the pH value of the buffer. As the pH increased, the intensities of the characteristic peaks and the crystallinity of Bi-EA gradually decreased. At pH 8, the crystalline structure of the material was almost completely lost, because the bismuth precursor was easily hydrolyzed in an aqueous solution [30]. Bismuth hydroxides are formed when the solution is more alkaline, thereby affecting the construction of open skeletons [31].

In addition to the pH level, the type of buffer also affected the synthesis of Bi-EA (Fig. S1, cf. Electronic Supplementary Material, ESM). The selection of non-coordinated buffer molecules during Bi-EA synthesis is critical to avoid the formation of complexes between bismuth ions and buffer molecules. Phosphate groups can strongly chelate metal ions [32,33], and Bi(III) cations are more inclined to combine with phosphate to generate $BiPO_4$ in phosphate buffered saline (PBS) (50 mmol·L^{-1}, pH 7) (Fig. S1). In addition, when the buffer solution contains chloride ions, bismuth oxychloride is generated instead of Bi-EA under the combined action of the pH and chloride ions (Tris-HCl and KCl-NaOH, Fig. S1). To avoid complexation between Bi(III) cations and buffer molecules, MES and HEPES with pH values of 6–7 were selected as buffer solutions. Both are Good's buffers and have the characteristics of high solubility in water, no complexation or precipitation with metal ions, a small salt effect, and chemical stability, among others [34,35]. Acetate radicals were also used as modulators for the synthesis of MOF materials, so acetate buffer with pH of 4–5 was selected as the buffer solution.

The morphology of Bi-EA synthesized at different pH values was studied using scanning electron microscopy (SEM) and are shown in Figs. 1 and S2 (cf. ESM). Typical Bi-EA synthesized in an aqueous solution containing acetic acid exhibited an irregular columnar morphology (Figs. 1(b) and S2(a)). In contrast, it presented a lamellar aggregation state in buffer solutions (Figs. 1(c–f) and S2(b–e)). The special chemical properties of Bi(III) cations and flexible coordination geometry make it easy to form layered materials [30]. When the pH value was 8, the composite lost its lamellar structure and appeared as fine particles (Fig. S2(f)), which was consistent with the X-ray diffraction (XRD) results.

Furthermore, the generation of Bi-EA was time dependent. Both bismuth acetate and EA were slightly soluble in water, and the assembly of Bi-EA and dissolution of the precursor in the reaction system were mutually facilitated, which was verified via electron microscopy combined with energy spectrum characterization (Fig. S3, cf. ESM). Unreacted EA was observed in the fibrous form when the reaction time was short (Figs. S3(a) and S3(b)). Elemental mapping characterization verified that bismuth was only distributed in the columnar or layered complexes (Fig. S3(d)). When the assembly was fully completed, Bi-EA exhibited a layered structure, and the bismuth elements were uniformly distributed in the material (Figs. S3(c), S3(e) and S3(f)). The time required for the preparation of Bi-EA could be adjusted by tuning the amount of precursor added. In the 10 mL system, the assembly of Bi-EA was completed in 5 h when the amounts of bismuth acetate and EA added were 30 and 10 mg, respectively.

3.2 Preparation and characterization of AMG@Bi-EA.

AMG was used as the model enzyme to evaluate the encapsulation effect of Bi-EA. The characterization of AMG@Bi-EA are shown in Fig. 2. As shown in Fig. 2(a), AMG@Bi-EA exhibited an irregular columnar or laminated morphology, which was different from that of the Bi-EA complex prepared under the same conditions. This may be due to the interactions between the enzymes and the metal/ligand. Enzyme encapsulation in Bi-EA was confirmed using the Bradford protein assay. The loading of AMG in the Bi-EA was calculated to be 3.6%. Furthermore, enzyme encapsulation was further confirmed using laser confocal microscopy. Fluorescein isothiocyanate-labeled AMG was used to prepare AMG@Bi-EA, and fluorescence signals indicated successful enzyme encapsulation (Fig. 2(b)). The corresponding bright field and merged images demonstrated that AMG was uniformly distributed in Bi-EA (Fig. S4, cf. ESM).

The specific surface areas and pore volumes of Bi-EA and enzyme@Bi-EA were analyzed using nitrogen adsorption and desorption experiments (Figs. 2(e) and 2(f)). Compared with Bi-EA, AMG@Bi-EA showed a significantly decreased specific surface area and pore volume, which may be due to the enzymes occupying the pores of Bi-EA. The specific surface area was decreased from 43.27 to 26.35 $m^2 \cdot g^{-1}$, and the pore volume was decreased from 0.1603 to 0.1287 $cm^3 \cdot g^{-1}$. These results indirectly indicated the successful encapsulation of the enzymes. TGA also confirmed the incorporation of enzymes in Bi-EA. As shown in Fig. 2(d), Bi-EA exhibited significant weight loss between 200 and 450 °C, which was mostly due to the degradation of EA ligands. Compared with pure Bi-EA, the weight loss of AMG@Bi-EA further increased. The thermogravimetric loss was roughly consistent with the enzymes loading results, which further indicated the successful preparation of AMG@Bi-EA. XRD confirmed that the addition of AMG did not change the topology of Bi-EA. However, the crystallinity of AMG@Bi-EA decreased slightly, which was mainly manifested by the decrease in the characteristic peak intensity and the broadening of the peak width. The initial AMG concentration did not substantially affecting the crystal form of the complex.

3.3 Biocatalytic activity and kinetic parameters of AMG@Bi-EA

AMG can hydrolyze starch to glucose, producing a

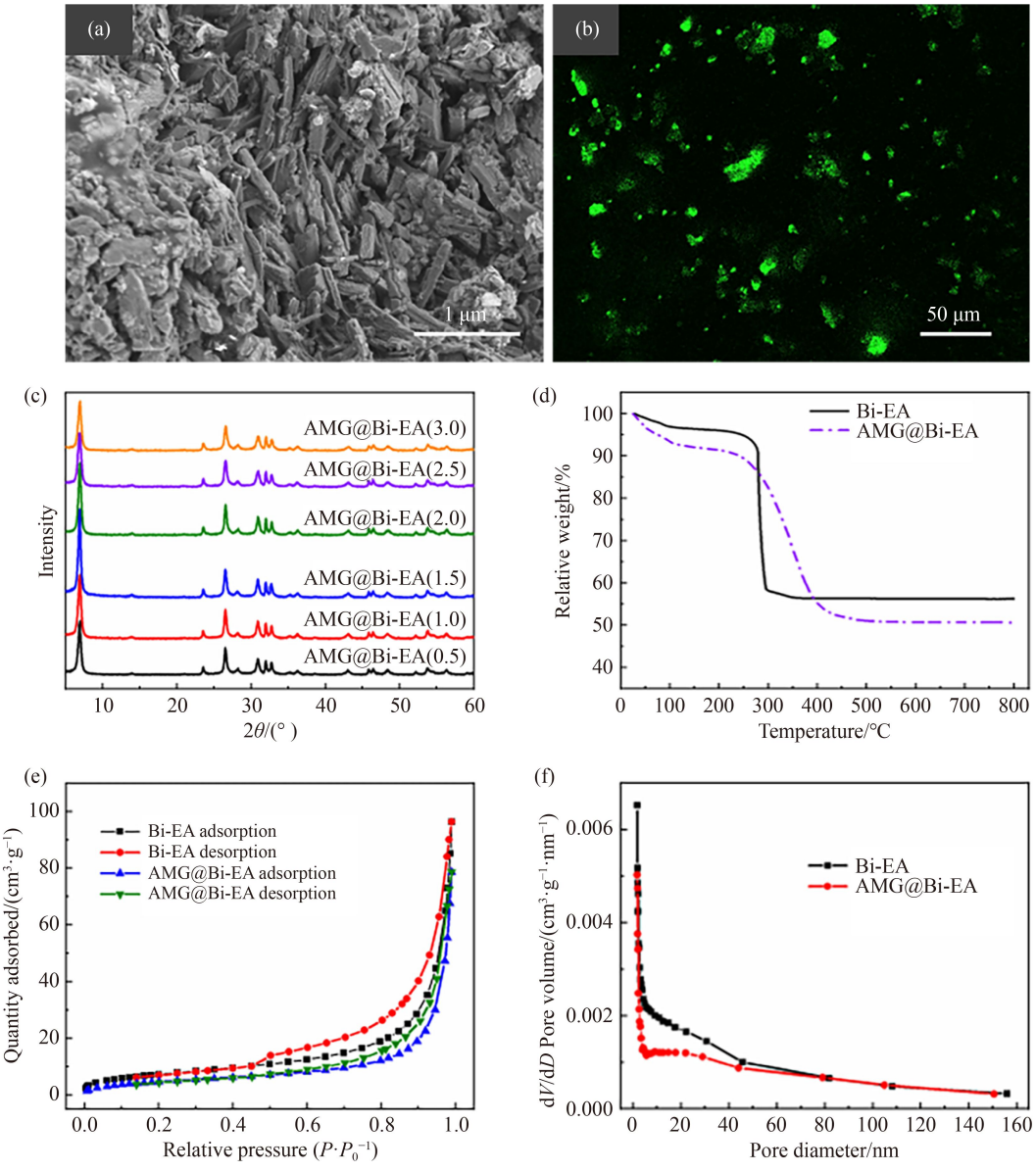

Fig. 2 Characterization of AMG@Bi-EA: (a) SEM image of AMG@Bi-EA; (b) laser confocal image of AMG@Bi-EA; (c) XRD pattern of AMG@Bi-EA with the addition of different AMG; (d) thermogravimetric analysis (TGA) curves of enzyme@Bi-EA and Bi-EA; (e) nitrogen adsorption and desorption isotherms of AMG@Bi-EA and Bi-EA; (f) their corresponding pore size distribution.

reducing terminal [36]. The activities of AMG and AMG@Bi-EA were measured using the DNS method [29]. Biocatalytic activity and kinetic parameters of AMG and AMG@Bi-EA are shown in Fig. 3. At the same enzyme content, AMG@Bi-EA achieved starch hydrolysis with a lower catalytic efficiency (Fig. 3(a)). After encapsulation, the specific activity of AMG@Bi-EA was calculated to be 48.92 ± 0.98 $U \cdot mg_{protein}^{-1}$, and the activity recovery was 11.8%. The relatively low activity recovery compared with the protein balance may be due to the limited porosity of AMG@Bi-EA, as evidenced by the N_2 isotherm. Poor porosity limits the entrance of the substrate and the transport of the product, resulting in reduced enzyme activity after encapsulation.

The hydrolysis rate of AMG catalyzed starch at different concentrations was also determined, and the kinetic constant was obtained via nonlinear fitting (Fig. 3(b)). The protein content of free AMG maintained during the determination of reaction kinetics parameters was consistent with that in AMG@Bi-EA. As can be seen in Table 1, the maximum reaction rate (V_{max}) of AMG catalyzed starch hydrolysis decreased from 10.78 to 3.643 $\mu mol \cdot L^{-1} \cdot min^{-1}$, which may be caused by mass transfer resistance. During co-precipitation, the enzyme may be buried in the enzyme@MOF complexes or partially exposed to the surface. Thus, the position of the enzyme in the complex may affect its catalytic function. For the small-molecule substrates that can diffuse into the pores of MOFs, enzymes buried in enzyme@MOF complexes can also combine with substrates to achieve

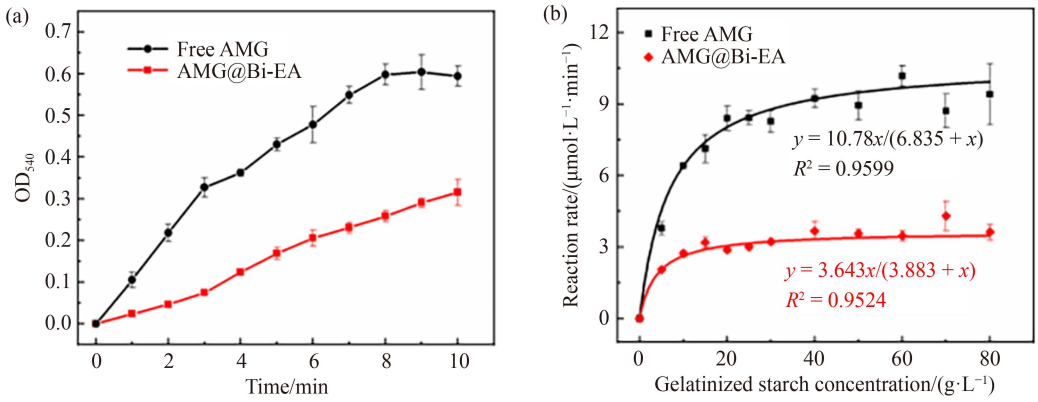

Fig. 3 (a) The catalytic activity and (b) enzymatic kinetics analysis of free amyloglucosidase and AMG@Bi-EA.

Table 1 Kinetic parameters of free AMG and AMG@Bi-EA

Enzyme	K_m/(g·L^{-1})	V_{max}/(μmol·L^{-1}·min^{-1})
Free AMG	6.835 ± 0.6142	10.78 ± 0.3880
AMG@Bi-EA	3.883 ± 0.4069	3.643 ± 0.0968

catalytic transformation. However, for macromolecular substrates, diffusion limitations make the surface-embedded enzymes the main contributors to catalysis [37,38]. Starch, as a macromolecular substrate, will have difficulty passing through the Bi-EA shell with poor porosity, and only AMG embedded in the surface layer showed catalytic activity, thus, V_{max} was significantly reduced. Although the overall catalytic rate of AMG@Bi-EA was reduced, it exhibited higher substrate affinity. During the co-precipitation process, the interaction between Bi-EA and AMG may provide a microenvironment, which is beneficial for maintaining the intrinsic dynamics or conformational freedom of the enzyme. These enhanced dynamics may be responsible for promoting the binding of the enzyme to the substrate. A similar phenomenon has been reported by Pan et al. [37]. However, the mechanisms underlying the interaction between enzymes and carriers during the encapsulation process requires further study to explain the changes in enzymes performance.

3.4 Acid-base stability of AMG@Bi-EA

To verify the stability of enzyme@Bi-EA in weak acid and base solutions, AMG@Bi-EA was soaked in a buffer with a pH value of 2–12 for a certain period, and its structural stability and activity retention are shown in Fig. 4. The variation in the optical density of AMG@Bi-EA over time during immersion is shown in Fig. 4(a). The OD_{540} of the sample did not decrease significantly after incubation for 10 h in the pH range of 2–10, indicating that the particles size of AMG@Bi-EA remained at the micron level. The stability of AMG@Bi-EA was further demonstrated using XRD. As shown in Fig. 4(b), the location of the characteristic peaks remained unchanged after incubating AMG@Bi-EA in buffers with different pH values (2–10), indicating no obvious changes in their crystal structures. The characteristic peaks were slightly shifted to a higher angle at pH of 12, which is consistent with the turbidity characterization. Interestingly, although it could not be prepared in the presence of phosphate, the structure of AMG@Bi-EA was stable in PBS buffer. The SEM images of AMG@Bi-EA also showed that its structure remained relatively intact (Fig. S5, cf. ESM). Compared with azolate or carboxylic acid ligand-based MOFs, which showed different degrees of decomposition under weakly acidic or weakly basic conditions, AMG@Bi-EA exhibited good acid-base stability, which was due to the strong chelation between polyphenols and metal ions [26–28].

The activity retention of AMG@Bi-EA was verified via incubation in buffers of different pH values. As shown in Fig. 4(c), except at a pH of 2, there was no obvious decrease in enzyme activity after immersing AMG@Bi-EA in the buffers with pH of 3–12 for 6 h, indicating that Bi-EA has a strong protective effect on AMG. For comparison, the stability of AMG encapsulated in ZIF-8 (AMG@ZIF-8) under weakly acidic conditions was also studied in the presence of proteinase K [30]. ZIF-8 is unstable under weakly acidic conditions (pH 6). During the decomposition of ZIF-8, the encapsulated enzymes leak out and are hydrolyzed by proteinase K, resulting in a loss of activity. As shown in Fig. 4(d), free AMG was almost completely inactivated after 3 h of incubation in the presence of proteinase K. AMG@Bi-EA retained 36.4% of its original activity, whereas AMG@ZIF-8 retained only 16.7%, which indicated that AMG@Bi-EA was more stable than AMG@ZIF-8.

3.5 Thermal stability of enzyme@Bi-EA

Enzymes are heat-sensitive, and high temperatures can damage their structure and cause irreversible inactivation [39,40]. The thermal stability of an enzyme can typically be improved via encapsulation. In this study, the thermal inactivation of free AMG and AMG@Bi-EA was

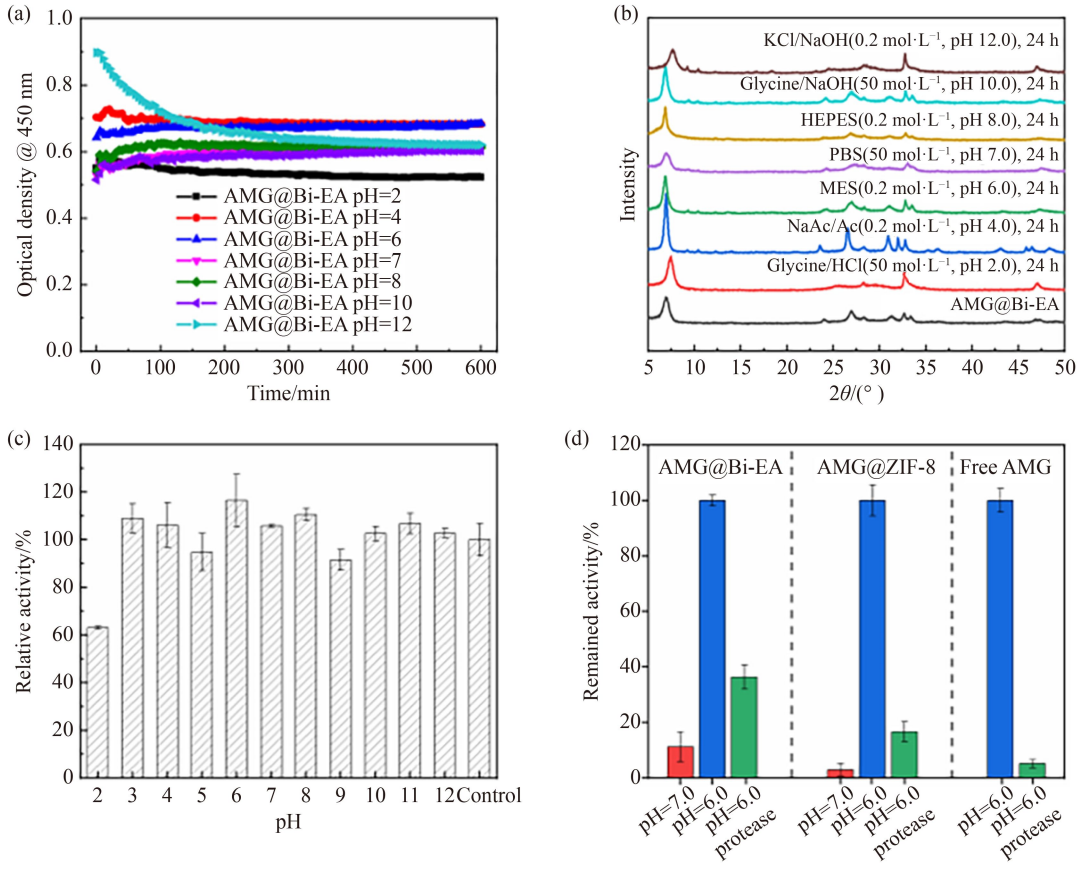

Fig. 4 (a) Turbidity and (b) XRD analysis of AMG@Bi-EA after immersion in buffers of different pH; (c) the activity of AMG@Bi-EA after immersion in buffers of different pH and (d) its stability in a weakly acidic solution in the presence of proteases.

analyzed and the results are shown in Fig. 5. Free AMG and AMG@Bi-EA were incubated at 60, 65, 70, 75, and 80 °C, and enzymatic activity was detected at 10-min intervals. The variation in residual activity with time is shown in Figs. 5(a) and 5(b). AMG@Bi-EA exhibited good thermal stability at 60–70 °C. After 1 h of incubation, AMG@Bi-EA retained 76.3%, 68.0% and 60.6% of its original activity; however, the free enzyme retained only 41.1%, 40.1%, and 13.7%, respectively. Both free AMG and AMG@Bi-EA were rapidly inactivated at 75 and 80 °C, respectively. Based on the variation in residual activity with time, the deactivation mechanical parameters and thermodynamic parameters of free AMG and AMG@Bi-EA were calculated using one-step deactivation model simulations (Figs. 5(c) and 5(d)) [41]. The thermal deactivation constant (k_d), $t_{1/2}$, and D-values for AMG and AMG@Bi-EA are listed in Table 2. The k_d of AMG@Bi-EA was much lower than that of free AMG at 60, 65, and 70 °C, and its $t_{1/2}$ and D-values increased approximately 3.0-, 2.4- and 4.5-fold, respectively. Furthermore, the inactivation energies of free AMG and AMG@Bi-EA were calculated using the Arrhenius equation (Figs. 5(e) and 5(f)). The E_d of AMG@Bi-EA was calculated to be 189.22 kJ·mol^{-1}, higher than that of free AMG (134.77 kJ·mol^{-1}). These results showed that the formation of AMG@Bi-EA could increase the tolerance temperature of AMG to 70 °C, also improved its thermal stability [42,43].

3.6 Reusability and storage stability of AMG@Bi-EA

Enzyme recycling is one of the targets of enzyme immobilization, which can significantly decrease the cost of enzyme usage. In this study, the reusability and storage stability of AMG@Bi-EA was also investigated and the results are shown in Fig. 6. As shown in Fig. 6(a), the activity of AMG@Bi-EA was retained at approximately 34% after ten repetitions, demonstrating its good reusability. The storage stability of free AMG and AMG@Bi-EA are shown in Fig. 6(b). After 20 days of storage, AMG@Bi-EA retained 72.3% of its original activity, whereas free AMG retained only 32.1% of its original activity. The good reusability and storage stability observed indicated that the encapsulation of Bi-EA provided stable enzyme protection, helping maintain enzymatic activity during multiple recoveries and long-term storage.

3.7 The versatility of Bi-EA for constructing enzyme@MOF complexes

The mild, selectable synthesis conditions and relatively short reaction time make Bi-EA a potential platform for

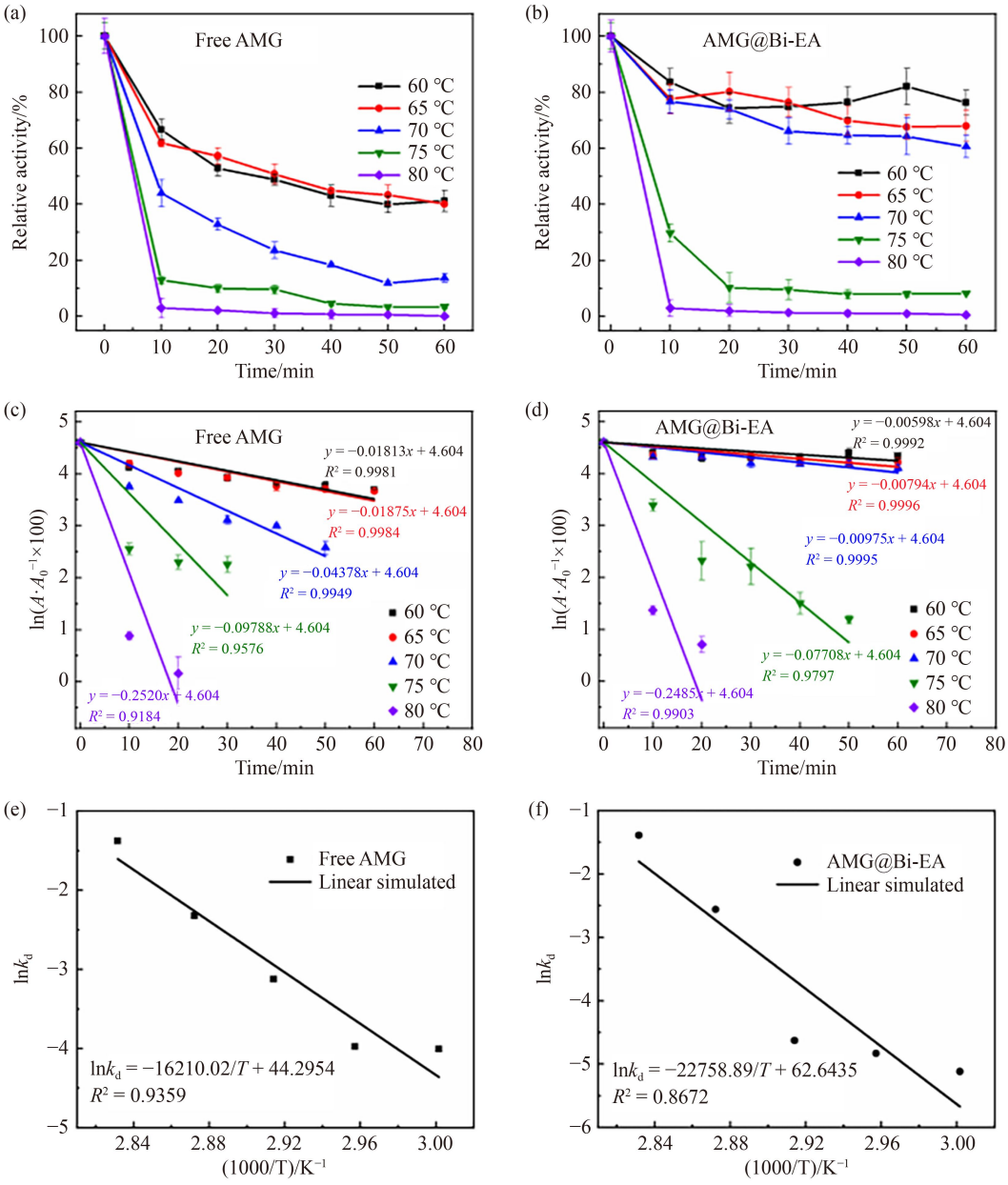

Fig. 5 (a, b) Thermal stability, (c, d) thermal inactivation kinetic studies and (e, f) Arrhenius plot for the inactivation of free AMG and AMG@Bi-EA.

Table 2 Thermal deactivation kinetic parameters of free AMG and AMG@Bi-EA

Paramcter	Free AMG					AMG@Bi-EA				
Temperature/°C	60	65	70	75	80	60	65	70	75	80
k_d/min^{-1}	0.0181	0.0188	0.0438	0.0979	0.252	0.00598	0.00794	0.00975	0.0771	0.249
$t_{1/2}$/min	38.23	36.97	15.83	7.08	2.75	115.90	87.29	71.09	8.99	2.79
D-value/min	127.03	122.83	52.60	23.53	9.14	385.12	290.05	236.21	29.88	9.27
E_d/(kJ·mol^{-1})	134.77					189.22				

immobilizing enzymes using a one-pot co-precipitation method. In addition to AMG, several other enzymes, such as CALB, OPH, GDH, GOx, and HRP, were used to verify the universality of this method. These enzymes have different properties such as molecular weight, isoelectric point, substrate size, and optimal pH range (Table S1, cf. ESM). The enzyme@MOF complexes preparation conditions were selected based on the optimum pH of the enzyme to avoid affecting enzyme activity. Bi-EA was synthesized in the pH range of 2–7.

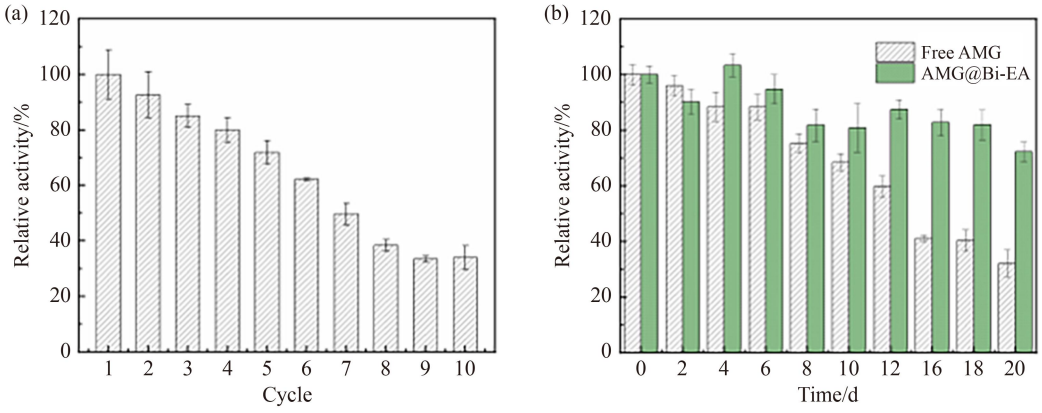

Fig. 6 (a) The reusability and (b) storage stability of AMG@Bi-EA.

For acid-sensitive enzymes, biocomposites were synthesized under neutral conditions. That indicated that Bi-EA could encapsulate different types of enzymes and enable interactions between encapsulated enzymes and cofactors, as well as between multiple enzymes.

Biocatalytic activity and kinetic parameters of CALB@Bi-EA and OPH@Bi-EA are shown in Figs. S6 and S7 (cf. ESM), respectively. The specific activity of CALB@Bi-EA was 1344.58 ± 65.49 $U \cdot g^{-1}$, while that of OPH@Bi-EA was 207.87 ± 15.35 $U \cdot g^{-1}$. Similar to AMG@Bi-EA, the K_m values of CALB@Bi-EA and OPH@Bi-EA decreased compared to their free forms (Table S2, cf. ESM). Their corresponding maximum catalytic rates also decreased to some extent, which may be due to the encapsulation of Bi-EA, limiting substrate delivery.

The activity recoveries of CALB@Bi-EA and OPH@Bi-EA were 48.9% and 68.2%, respectively, which are higher than AMG@Bi-EA. When the original protein concentration was 1 $mg \cdot mL^{-1}$, the encapsulation efficiencies of Bi-EA for AMG, CALB and OPH were 13.1%, 78.6% and 97.8%, respectively. Their zeta potentials indicated that the encapsulation efficiency may be related to the surface charge of the enzyme. As shown in Fig. S8 (cf. ESM), AMG, CALB, and OPH were all negatively charged in the buffer used, and their electronegativity increased sequentially. During the co-precipitation of enzymes and ligands, it is possible that the enzymes bound to the positively charged Bi^{3+} cation first, and then doped into the composite during the assembly of bismuth with EA. Therefore, a higher electronegativity on the enzyme surface makes it easier to encapsulate into the composite, thus exhibiting a higher activity recovery, similar to the encapsulation of enzymes in ZIF-8 [44,45].

GDH was used to evaluate the effect of Bi-EA encapsulation on cofactor-dependent enzymes. As shown in Fig. S9 (cf. ESM), interactions between enzymes and nicotinamide adenine dinucleotide (NAD^+) could still happen after encapsulation. The kinetic characteristics of free GDH and GDH@Bi-EA were then determined by varying the NAD^+ concentration at a fixed glucose dosage. The K_m values of GDH for NAD^+ were essentially unchanged before and after immobilization, but a significant decrease in V_{max} was observed, which could be due to reticulation limitation and/or impeded mass transfer [46].

A cascade reaction between GOx and HRP was also used to test the effect of Bi-EA encapsulation on the two enzymes. As shown in Fig. S10 (cf. ESM), the cascade reaction between GOx and HRP still occurred after encapsulation, and glucose was colorimetrically detected. In the presence of GOx and HRP@Bi-EA, the absorbance values at 415 nm showed good linearity when the glucose was 0–2000 $\mu mol \cdot L^{-1}$. The detection limit of this method was 3.028 $\mu mol \cdot L^{-1}$.

4 Conclusions

In summary, a universal enzyme immobilization platform was constructed by encapsulating enzymes in Bi-EA. The stability of the enzymes was enhanced after encapsulation in Bi-EA, and multiple recycling of the enzyme@Bi-EA was achieved. Remarkably, enzyme@Bi-EA remained stable over a wide pH range (2–12), making the method adaptable for immobilizing different enzymes for catalyzing reactions under optimal pH conditions. The green and harmless precursor source, mild and simple preparation process and robust acid-base stability provided a versatile strategy for preparing enzyme@MOF complexes, facilitating the application of MOFs in biocatalysis.

Acknowledgements This work was financially supported by the National Natural Science Foundation of China (Grant Nos. 22178083, 22078081 and 21878068), the Natural Science Foundation of Tianjin China (Grant No. 20JCYBJC00530), the Hebei Key Research and Development Project (Grant No. 20372802D), Open Funding Project of the State Key Laboratory of Biocatalysis and Enzyme Engineering (Grant No. SKLBEE2020011), Science Technology Research Project of Higher Education of Hebei Province (Grant No. QN2021045) and Tianjin Enterprise Science and Technology Commissioner Project (Grant No. 21YDTPJC00810).

Electronic Supplementary Material Supplementary material is available in the online version of this article at https://dx.doi.org/10.1007/s11705-022-2278-4 and is accessible for authorized users.

References

1. Wu S, Snajdrova R, Moore J C, Baldenius K, Bornscheuer U T. Biocatalysis: enzymatic synthesis for industrial applications. Angewandte Chemie International Edition, 2021, 60(1): 88–119
2. Rodrigues R C, Berenguer-Murcia A, Carballares D, Morellon-Sterling R, Fernandez-Lafuente R. Stabilization of enzymes via immobilization: multipoint covalent attachment and other stabilization strategies. Biotechnology Advances, 2021, 52: 107821
3. Wiltschi B, Cernava T, Dennig A, Galindo Casas M, Geier M, Gruber S, Haberbauer M, Heidinger P, Herrero Acero E, Kratzer R, Luley-Goedl C, Müller C A, Pitzer J, Ribitsch D, Sauer M, Schmölzer K, Schnitzhofer W, Sensen C W, Soh J, Steiner K, Winkler C K, Winkler M, Wriessnegger T. Enzymes revolutionize the bioproduction of value-added compounds: from enzyme discovery to special applications. Biotechnology Advances, 2020, 40: 107520
4. Jemli S, Ayadi-Zouari D, Hlima H B, Bejar S. Biocatalysts: application and engineering for industrial purposes. Critical Reviews in Biotechnology, 2016, 36(2): 246–258
5. Bell E L, Finnigan W, France S P, Green A P, Hayes M A, Hepworth L J, Lovelock S L, Niikura H, Osuna S, Romero E, Ryan K S, Turner N J, Flitsch S L. Biocatalysis. Nature Reviews Methods Primers, 2021, 1(1): 46
6. Sheldon R A, Pelt S V. Enzyme immobilisation in biocatalysis: why, what and how. Chemical Society Reviews, 2013, 42(15): 6223–6235
7. Finnigan W, Hepworth L J, Flitsch S L, Turner N J. RetroBioCat as a computer-aided synthesis planning tool for biocatalytic reactions and cascades. Nature Catalysis, 2021, 4(2): 98–104
8. Santos A G, da Rocha G O, de Andrade J B. Occurrence of the potent mutagens 2-nitrobenzanthrone and 3-nitrobenzanthrone in fine airborne particles. Scientific Reports, 2019, 9(1): 1–13
9. Garcia-Galan C, Berenguer-Murcia A, Fernandez-Lafuente R, Rodrigues R C. Potential of different enzyme immobilization strategies to improve enzyme performance. Advanced Synthesis & Catalysis, 2011, 353(16): 2885–2904
10. Sheldon R A, Basso A, Brady D. New frontiers in enzyme immobilisation: robust biocatalysts for a circular bio-based economy. Chemical Society Reviews, 2021, 50(10): 5850–5862
11. Wu X, Hou M, Ge J. Meta-organic frameworks and inorganic nanoflowers: a type of emerging inorganic crystal nanocarrier for enzyme immobilization. Catalysis Science & Technology, 2015, 5(12): 5077–5085
12. Cui J, Ren S, Sun B, Jia S. Optimization protocols and improved strategies for metal–organic frameworks for immobilizing enzymes: current development and future challenges. Coordination Chemistry Reviews, 2018, 370: 22–41
13. Liu J, Liang J, Xue J, Liang K. Metal–organic frameworks as a versatile materials platform for unlocking new potentials in biocatalysis. Small, 2021, 17(32): e2100300
14. Wang X, Lan P, Ma S. Metal–organic frameworks for enzyme immobilization: beyond host matrix materials. ACS Central Science, 2020, 6(9): 1497–1506
15. Gkaniatsou E, Sicard C, Ricoux R, Mahy J P, Steunou N, Serre C. Metal–organic frameworks: a novel host platform for enzymatic catalysis and detection. Materials Horizons, 2017, 4(1): 55–63
16. Liang K, Ricco R, Doherty C M, Styles M J, Bell S, Kirby N, Mudie S, Haylock D, Hill A J, Doonan C J, Falcaro P. Biomimetic mineralization of metal–organic frameworks as protective coatings for biomacromolecules. Nature Communications, 2015, 6(1): 7240
17. Huang W, Zhang W, Gan Y, Yang J, Zhang S. Laccase immobilization with metal–organic frameworks: current status, remaining challenges and future perspectives. Critical Reviews in Environmental Science and Technology, 2020, 52, 7: 1282–1324
18. Tong L, Huang S, Shen Y, Liu S, Ma X, Zhu F, Chen G, Ouyang G. Atomically unveiling the structure-activity relationship of biomacromolecule-metal–organic frameworks symbiotic crystal. Nature Communications, 2022, 13(1): 951
19. Huang S, Chen G, Ouyang G. Confining enzymes in porous organic frameworks: from synthetic strategy and characterization to healthcare applications. Chemical Society Reviews, 2022, 51(15): 6824–6863
20. Li Z, Wang L, Qin L, Lai C, Wang Z, Zhou M, Xiao L, Liu S, Zhang M. Recent advances in the application of water-stable metal–organic frameworks: adsorption and photocatalytic reduction of heavy metal in water. Chemosphere, 2021, 285: 131432
21. He T, Kong X J, Li J R. Chemically stable metal–organic frameworks: rational construction and application expansion. Accounts of Chemical Research, 2021, 54(15): 3083–3094
22. Guo Y, Sun Q, Wu F, Dai Y, Chen X. Polyphenol-containing nanoparticles: synthesis, properties, and therapeutic delivery. Advanced Materials, 2021, 33(22): e2007356
23. Lin Z, Zhou J, Cortez-Jugo C, Han Y, Ma Y, Pan S, Hanssen E, Richardson J J, Caruso F. Ordered mesoporous metal-phenolic network particles. Journal of the American Chemical Society, 2020, 142(1): 335–341
24. Ejima H, Richardson J J, Caruso F. Metal-phenolic networks as a versatile platform to engineer nanomaterials and biointerfaces. Nano Today, 2017, 12: 136–148
25. Chen E, Qiu M, Zhang Y, Zhu Y, Liu L, Sun Y, Bu X, Zhang J, Lin Q. Acid and base resistant zirconium polyphenolate-metalloporphyrin scaffolds for efficient CO_2 photoreduction. Advanced Materials, 2018, 30(2): 1704388
26. Ismail M, Bustam M A, Yeong Y F. Gallate-based metal–organic frameworks, a new family of hybrid materials and their applications: a review. Crystals, 2020, 10(11): 1006
27. Chiong J A, Zhu J, Bailey J B, Kalaj M, Subramanian R H, Xu W, Cohen S M, Tezcan F A. An exceptionally stable metal–organic framework constructed from chelate-based metal–organic polyhedra. Journal of the American Chemical Society, 2020, 142(15): 6907–6912
28. Grape E S, Flores J G, Hidalgo T, Martinez-Ahumada E, Gutierrez-Alejandre A, Hautier A, Williams D R, O'Keeffe M, Ohrstrom L, Willhammar T, Horcajada P, Ibarra I A, Inge A K. A robust and biocompatible bismuth ellagate MOF synthesized under green ambient conditions. Journal of the American Chemical Society, 2020, 142(39): 16795–16804

29. Miller G N. Use of dinitrosaIicyIic acid reagent for determination of reducing sugar. Analytical Chemistry, 1959, 81(3): 426–428
30. Wang Z, Zeng Z, Wang H, Zeng G, Xu P, Xiao R, Huang D, Chen S, He Y, Zhou C, Cheng M, Qin H. Bismuth-based metal–organic frameworks and their derivatives: opportunities and challenges. Coordination Chemistry Reviews, 2021, 439: 2139052
31. Yang N, Sun H. Biocoordination chemistry of bismuth: recent advances. Coordination Chemistry Reviews, 2007, 251(17-20): 2354–2366
32. Wang L, Wang Y, He R, Zhuang A, Wang X, Zeng J, Hou J. A new nanobiocatalytic system based on allosteric effect with dramatically enhanced enzymatic performance. Journal of the American Chemical Society, 2013, 135(4): 1272–1275
33. Jiang Z, Chen Y, Xing M, Ji P, Feng W. Fabrication of a fibrous metal–organic framework and simultaneous immobilization of enzymes. ACS Omega, 2020, 5(36): 22708–22718
34. Good N E, Winget G D, Winter W, Connolly T N, Izawa S, Singh R M. Hydrogen ion buffers for biological research. Biochemistry, 1966, 5(2): 467–477
35. Colwell K A, Jackson M N, Torres-Gavosto R M, Jawahery S, Vlaisavljevich B, Falkowski J M, Smit B, Weston S C, Long J R. Buffered coordination modulation as a means of controlling crystal morphology and molecular diffusion in an anisotropic metal–organic framework. Journal of the American Chemical Society, 2021, 143(13): 5044–5052
36. Fogarty W M, Benson C P. Purification and properties of a thermophilic amyloglucosidase from *Aspergillus nige*. European Journal of Applied Microbiology and Biotechnology, 1983, 18(5): 271–278
37. Pan Y, Li Q, Li H, Farmakes J, Ugrinov A, Zhu X, Lai Z, Chen B, Yang Z. A general Ca-MOM platform with enhanced acid-base stability for enzyme biocatalysis. Chem Catalysis, 2021, 1(1): 146–161
38. Pan Y, Li H, Farmakes J, Xiao F, Chen B, Ma S, Yang Z. How do enzymes orient when trapped on metal–organic framework (MOF) surfaces? Journal of the American Chemical Society, 2018, 140(47): 16032–16036
39. Owusu R K, Makhzoum A, Knapp J S. Heat inactivation of lipase from psychrotrophic *Pseudomonas fluorescens* P38: activation parameters and enzyme stability at low or ultra-high temperatures. Food Chemistry, 1992, 44(4): 261–268
40. Pietricola G, Ottone C, Fino D, Tommasi T. Enzymatic reduction of CO_2 to formic acid using FDH immobilized on natural zeolite. Journal of CO_2 Utilization, 2020, 42: 101343
41. Tang Y, Li W, Muhammad Y, Jiang S, Huang M, Zhang H, Zhao Z, Zhao Z. Fabrication of hollow covalent-organic framework microspheres via emulsion-interfacial strategy to enhance laccase immobilization for tetracycline degradation. Chemical Engineering Journal, 2021, 421: 129743
42. Patil P D, Yadav G D. Rapid in situ encapsulation of laccase into metal–organic framework support (ZIF-8) under biocompatible conditions. ChemistrySelect, 2018, 3(17): 4669–4675
43. de Castro R J S, Ohara A, Nishide T G, Albernaz J R M, Soares M H, Sato H H. A new approach for proteases production by *Aspergillus niger* based on the kinetic and thermodynamic parameters of the enzymes obtained. Biocatalysis and Agricultural Biotechnology, 2015, 4(2): 199–207
44. Chen G, Kou X, Huang S, Tong L, Shen Y, Zhu W, Zhu F, Ouyang G. Modulating the biofunctionality of metal–organic-framework-encapsulated enzymes through controllable embedding patterns. Angewandte Chemie International Edition, 2020, 59(7): 2867–2874
45. Maddigan N K, Tarzia A, Huang D M, Sumby C J, Bell S G, Falcaro P, Doonan C J. Protein surface functionalisation as a general strategy for facilitating biomimetic mineralisation of ZIF-8. Chemical Science, 2018, 9(18): 4217–4123
46. Hsu P H, Chang C C, Wang T H, Lam P K, Wei M Y, Chen C T, Chen C Y, Chou L Y, Shieh F K. Rapid fabrication of biocomposites by encapsulating enzymes into Zn-MOF-74 via a mild water-based approach. ACS Applied Materials & Interfaces, 2021, 13(44): 52014–52022